Marangoni-induced actuation of miscible liquid droplets on an incline

Vi-Vie Ng[a], Mathieu Sellier[a,*], Volker Nock[b]

[a]*Department of Mechanical Engineering, University of Canterbury, Private Bag 4800, Christchurch, 8140, New Zealand*

[b]*Department of Electrical and Computer Engineering, University of Canterbury, Private Bag 4800, Christchurch, 8140, New Zealand*

*Corresponding author.

E-mail addresses: vivienne.ng@pg.canterbury.ac.nz (V. Ng), mathieu.sellier@canterbury.ac.nz (M. Sellier), volker.nock@canterbury.ac.nz (V.Nock)

ABSTRACT

This paper reports on the self-propulsion of a droplet up an incline, confined on a polydimethylsiloxane (PDMS) channel rendered hydrophilic through combined oxygen plasma and polyvinylpyrrolidone (PVP) treatment. Our work investigates the effects of substrate angle on the distance traveled, along with the threshold value for when gravitational force overcomes Marangoni force. A numerical simulation has been developed, where the governing equations solved using COMSOL validated our experimental findings. The numerical simulation, made dimensionless, allows for the prediction of distance traveled and droplet morphology when key parameters in a physical experiment are varied.

Keywords: Marangoni, droplet propulsion, incline, PVP

1. Introduction

Self-propulsion of droplets may facilitate automated synthesis and analysis of small liquid samples in lab-on-a-chip applications. Various techniques of droplet self-propulsion have been studied: (a) chemical treatment of substrates to induce wettability gradients (Greenspan, 1978; Brochard, 1989; Chaudhury and Whitesides, 1992), (b) temperature gradients to induce surface tension differences (Ford and Nadim, 1994; Smith, 1995; Darhuber et al., 2003), (c) the use of surfactants to induce surface tension gradients (Dos Santos and Ondarçuhu, 1995; Yarin et al., 2002), (d) electrowetting on dielectrics (EWOD) (Moon et al., 2002; Yeo and Chang, 2005) and (e) surface acoustics waves (SAW) produced by piezoelectric materials (Ding et al., 2013; Yeo and Friend, 2014). Though each of these methods presents its own advantages, some of its drawbacks include: (a) the need for external power sources, (b) unsustainable wettability gradients, and (c) complex microfabrication processes. Building upon previous work by our group (Sellier et al., 2011, 2013), we further explore the feasibility of droplet translation up an incline surface through coalescence-induced self-propulsion.

To date, several works pertaining to the motion of micro-sized droplets moving uphill have been published. By exposing silicon with the vapor of decyltrichlorosilane to create a surface energy gradient, Chaudhury and Whitesides (1992) showed a droplet moving uphill on a 15^{o} inclined surface. (Bain et al., 1994) and (Chandesris et al., 2013) fabricated grooves with a wettability gradient to induce motion, on a glass and a silicon surface respectively. (Vorobyev and Guo, 2010) demonstrated a droplet moving vertically on a superwicking glass by means of grooves created using laser beams. Using microwave-plasma enhanced chemical vapor deposition (MPECVD) to create a superhydrophobic thin film on glass, (Wu et al., 2006) showed a water droplet moving up a 17^{o} incline after the substrate was charged with static electricity.

Based on high chemical gradient, (Yao et al., 2012) showed that a hydrofluoric acid droplet propels itself by etching the silicon substrate underneath on inclines of 15^o, 45^o, and 90^o. In addition to wettability gradients, (Zhang and Han, 2007) included shape-gradients in their cleaved mica substrate and showed uphill movement up to an angle of 15^o.

Our work is different in that we do not involve complex and time-consuming microfabrication processes such as photolithography, etching, etc. Also, most reported works on droplet moving uphill are done on rigid surfaces such as silicon wafers, glass, stainless steel and mica. Our choice of using a flexible elastomer that is polydimethylsiloxane (PDMS) offers several advantages: Since it is liquid before being heat-cured, it can be poured onto designed molds to create substrates with custom surface features down to the nanometer range if required. The thickness of PDMS substrates can be easily controlled by adjusting the volume of pre-polymer cast or by spin-coating the pre-polymer onto other materials. PDMS is transparent at optical wavelengths (240 nm – 1100 nm), which eases the inspection of the contents in droplets on the surface both visually and under a microscope. It has low auto-fluorescence (Piruska et al., 2005), which facilitates biochemical assays involving fluorescence signals. Furthermore, its nontoxicity and biocompatibility make it suitable for lab-on-a-chip applications pertaining to biological entities such as cells and microorganisms (Kim et al., 2011). Also, it is inexpensive compared to silicon. Our choice of material and mechanism in guiding a droplet along a hydrophilic channel is well-suited for various digital microfluidics applications (Nock et al., 2013).

In comparison to previous works, which rely on surface energy gradients engineered either onto a substrate, or between a droplet and the underlying substrate, our work proposes the introduction of a surface energy gradient through liquid-vapor phase interaction, as well as from

the direct mixing of two miscible liquids on a substrate. We first present in Section 2 the theoretical framework used in simulating our experimental observation, leading to the governing equations used for numerical analysis. A thorough description of the experimental procedure is presented in Section 3. The results and analyses from our experiment and numerical simulations are reported in Section 4.

2. Theoretical simulation

Our theoretical simulation begins with defining a parabolic droplet with height h_o, and characteristic radius R_o, resting on an inclined plane at an angle α, as shown in Fig. 1(a). The direction of flow is constrained to the x-direction only, on a hydrophilic stripe of width w, as illustrated in Fig. 1(b). The system studied consists of a droplet of water, which is actuated by a droplet of ethanol (EtOH). A video of the resulting phenomenon can be viewed at http://www.scivee.tv/node/63808.

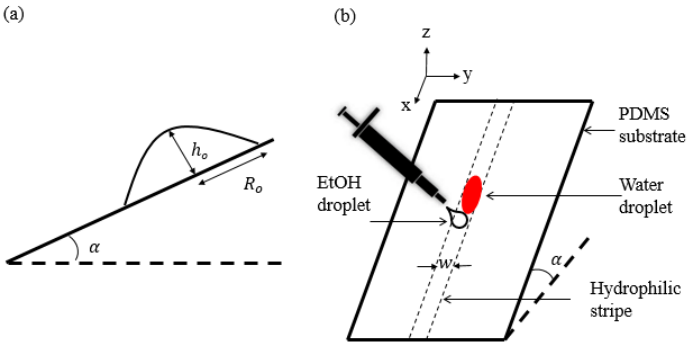

Fig. 1. An illustration of (a) a water droplet resting on an incline, and (b) a schematic of the EtOH droplet deposited adjacent to the water droplet resting on an incline.

In simulating the behavior of droplet flow on an inclined homogeneous or heterogeneous surface, we invoke a set of governing equations as follows (Sellier et al., 2011):

$$\frac{\partial h}{\partial t} = -\frac{\partial q_x}{\partial x}, \tag{1}$$

$$q_x = -\frac{h^3}{3\mu}\left(\frac{\partial p}{\partial x} - \rho g sin\alpha\right) + \frac{\tau h^2}{2\mu}, \tag{2}$$

$$p = -\gamma\left(\frac{\partial^2 h}{\partial x^2} + \frac{\partial^2 h}{\partial y^2}\right) - \Pi, \tag{3}$$

$$\frac{\partial ch}{\partial t} = -\frac{\partial}{\partial x}(cq_x) + D\frac{\partial}{\partial x}\left(h\frac{\partial c}{\partial x}\right), \tag{4}$$

where $h(x, y, t)$ is the droplet thickness normal to the substrate, q_x is the discharge, $p(x, y, t)$ is the pressure, γ is the surface tension, μ is the dynamic viscosity, $c(x, y, t)$ is the local concentration of EtOH and D is the diffusivity constant. For a uni-directional flow in the x-direction, the conservation of mass equation reduces to Eq. (1). The discharge expressed in Eq. (2) incorporates a pressure gradient, and a surface tension gradient represented by τ. Eq. (3) accounts for the balance of normal stresses at the small slope interface (Darhuber et al., 2003) with a disjoining pressure term, Π incorporated to remove the contact line singularity. Eq. (4)

describes the conservation of the EtOH in the system. We further define the dependent variables in the governing equations as follows:

$$\Pi(h, h^*) = B\left[\left(\frac{h^*}{h}\right)^n - \left(\frac{h^*}{h}\right)^m\right], \tag{5}$$

$$h(x, y, t) = h_c(x, t)\left(1 - \frac{4y^2}{w^2}\right), \tag{6}$$

$$c = \frac{h_1}{h}, \tag{7}$$

$$\tau = -\frac{\partial \gamma}{\partial c}.\frac{\partial c}{\partial x}, \tag{8}$$

for which the disjoining pressure term in Eq. (5) is a function of the precursor film of thickness h^*; a height h represented by both a centerline height, h_c and a width, w as expressed in Eq. (6), and a constant $B = \gamma(n-1)(m-1)(1-\cos\theta_0)/h^*(n-m)$, where $(n, m) = (3,2)$ are the exponents of the interaction potential, and θ_0 the equilibrium contact angle. The precursor thin film, h^* is introduced to remove the stress singularity occurring in problems with a moving contact line. According to Darhuber et al. (2003), if the width of the stripe is much smaller than the capillary length of the droplet, i.e. $w \ll l_c$, the droplet adopts a parabolic profile, resulting in an expression for droplet thickness as in Eq. (6). A fictitious EtOH height h_1 introduced in Eq. (7) is to be substituted for the surface tension expression in Eq. (8). Using these derivations and

integrating Eq. (2) and Eq. (3) over the width of the stripe, i.e. from $-w/2$ to $w/2$, we obtain an expression for the discharge as

$$Q_x = -\frac{h_c^3}{3\mu} w \left(\frac{\partial p}{\partial x} - \rho g sin\alpha\right) - \frac{1}{\mu}\frac{\partial \gamma}{\partial c}\frac{4w}{15}\left(h_c \frac{\partial h_1}{\partial x} - h_1 \frac{\partial h_c}{\partial x}\right), \tag{9}$$

and an expression for capillary pressure as

$$p = -\gamma\left(\frac{128}{315}\frac{\partial^2 h_c}{\partial x^2} - \frac{128}{35w^2}h_c\right) - B\left[\left(\frac{h^*}{h_c}\right)^2 - \frac{2}{3}\left(\frac{h^*}{h_c}\right)^3\right]. \tag{10}$$

Similarly, Eq. (4) can now be written as

$$\frac{2w}{3}\frac{\partial h_1}{\partial t} = -\frac{\partial}{\partial x}\left(\frac{h_1}{h_c}Q_x\right) + D\frac{2w}{3}\frac{\partial}{\partial x}\left(\frac{\partial h_1}{\partial x} - \frac{h_1}{h_c}\frac{\partial h_c}{\partial x}\right). \tag{11}$$

By substituting these variables:

$$\tilde{h}_c = \frac{h_c}{h_0}, \tilde{h}_1 = \frac{h_1}{h_0}, \tilde{x} = \frac{x}{l_0}, \tilde{p} = \frac{p}{p_0}, \tilde{c} = \frac{c}{c_0}, \tilde{t} = \frac{t}{t_0} \text{ and } \tilde{\gamma} = \frac{\gamma}{\gamma_0}, \tag{12}$$

along with the scales $P_0 = \frac{\gamma_0 h_0}{l_0^2}$, $T_0 = \frac{3\mu l_0^2}{P_0 h_0^2}$, and $\varepsilon = \frac{h_0}{l_0}$ we obtain the following dimensionless governing equations:

$$\frac{2}{3}\frac{\partial \tilde{h}_c}{\partial \tilde{t}} + \frac{\partial}{\partial \tilde{x}}\left\{-\tilde{h}_c^3\left(\frac{\partial \tilde{p}}{\partial \tilde{x}} - \frac{16}{35}\frac{B_0 sin\alpha}{\varepsilon}\right) + \Sigma\left(\tilde{h}_c\frac{\partial \tilde{h}_1}{\partial \tilde{x}} - \tilde{h}_1\frac{\partial \tilde{h}_c}{\partial \tilde{x}}\right)\right\} = 0, \quad (13)$$

$$\tilde{p} + \frac{128}{315}\tilde{\gamma}\frac{\partial^2 \tilde{h}_c}{\partial \tilde{x}^2} - \frac{128}{35}\frac{l_0^2}{w^2}\tilde{\gamma}\tilde{h}_c = -B\frac{l_0^2}{h_0\gamma_0}\left[\left(\frac{\tilde{h}^*}{\tilde{h}_c}\right)^n - \frac{2}{3}\left(\frac{\tilde{h}^*}{\tilde{h}_c}\right)^m\right], \quad (14)$$

$$\frac{2}{3}\frac{\partial \tilde{h}_1}{\partial \tilde{t}} + \frac{\partial}{\partial \tilde{x}}\left\{-\tilde{h}_c^2\tilde{h}_1\left(\frac{\partial \tilde{p}}{\partial \tilde{x}} - \frac{16}{35}\frac{B_0 sin\alpha}{\varepsilon}\right) + \Sigma\left(\tilde{h}_1\frac{\partial \tilde{h}_1}{\partial \tilde{x}} - \frac{\tilde{h}_1^2}{\tilde{h}_c}\frac{\partial \tilde{h}_c}{\partial \tilde{x}}\right) - d\left(\frac{\partial \tilde{h}_1}{\partial \tilde{x}} - \frac{\tilde{h}_1}{\tilde{h}_c}\frac{\partial \tilde{h}_c}{\partial \tilde{x}}\right)\right\} = 0, \quad (15)$$

where $B_0 = \frac{\rho g l_0^2}{\gamma_0}$ represents the Bond number, $\Sigma = -\frac{\partial \tilde{\gamma}}{\partial \tilde{c}}\frac{4}{5}\frac{1}{c_0\varepsilon^2}$ and $d = \frac{2D\mu}{h_0\gamma_0\varepsilon^2}$. These equations were solved in the commercial Finite Element package COMSOL 5.0.

3. Materials and methods

We analyzed the movement of droplets on flat PDMS substrates inclined at various angles. The PDMS substrates were prepared by replica-casting. In brief, PDMS pre-polymer was first prepared by mixing the base and curing agents (Sylgard 184, Dow Corning) at 10:1 w/w ratio, followed by degassing of the mixture in a desiccator until no air bubbles were visible. The liquid pre-polymer was then poured into single-well polystyrene (PS) cell culture trays (Thermo Scientific) to yield flat PDMS substrates of approximately 5 mm thickness. Subsequent curing was carried out on a hotplate for 6 h at 80 °C. The PDMS substrates were left to cool at room temperature for 24 h before being carefully peeled out of the PS tray. To ensure surface planarity, only the side that was in contact with the PS tray was used for the experiments; this side takes on the surface roughness of the PS tray, which has an RMS value of ~ 6 nm (Zeiger et

al., 2013). Because of the observed symmetry upon droplet deposition on this surface, we may assume that our substrate did not significantly impact our experiments. Prior to use, the substrates were stored sandwiched between clean polyethylene (PE) sheets.

Hydrophilic traces measuring 1 mm wide were created on the cured PDMS substrates using cut-out PE strips. This strips were used to protect the native PDMS surface underneath from subsequent plasma exposure. To ensure good adherence, the back of a pair of tweezers was used in a gliding motion to manually attach the PE strips onto the PDMS substrate. The entire assembly was then loaded into a barrel plasma etcher (Emitech K1050X, Quorum) for O_2 plasma exposure lasting 3 minutes at 30 W RF power. Immediately after plasma exposure the PDMS was then treated with polyvinylpyrrolidone (PVP) (Sigma-Aldrich) according to the procedures reported by (Hemmilä et al., 2012). The treated substrates were kept in a controlled environment where also prior preparations and subsequent experiments were performed: 21 ^{o}C +/- 1 ^{o}C and 50% humidity.

Individual rectangular PDMS pieces measuring 2 × 4 cm, with a 1 mm wide, now hydrophilic trace in the middle, were cut from the treated PDMS substrates. These rectangular pieces were set on a piece of glass attached in perpendicular to an adjustable triangle compass. Fig. 2 shows the experimental setup. Propulsion experiments were then carried out at angles 0^{o} to 24^{o}, with increments of 4^{o}.

For each experiment first a water droplet of volume 1 µl was deposited onto the trace using an electronic multi-channel micropipette (0.2-10 µl Picus, Biohit). This was followed by deposition of a 1 µl EtOH droplet adjacent to the water droplet. The experiment was simultaneously recorded using a high-speed digital camera (MQ013MG-E2, Ximea) connected

to a PC via USB-3 interface. Recorded images were analyzed using the Image Processing toolbox in Matlab (R2013b, Mathworks).

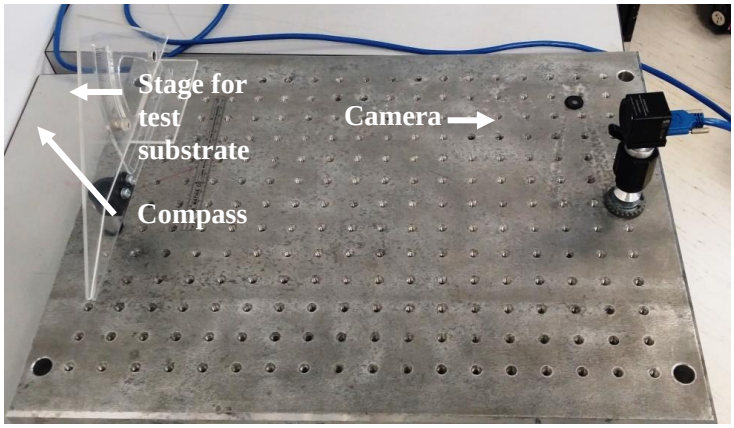

Fig. 2. Setup of the experiment showing the triangle compass with attached substrate stage and digital camera used for observation of droplet translation.

The side-view depicting droplet translation up an incline is shown in Fig. 3. The overlaid images analyzed using Image J 1.49 (Rasband, 1997) show the green droplet as the starting position, and the red droplet as the final position. To further aid observation, the insets show close-ups of the droplets. Subsequent measurements of propulsion distance from the selected images were carried out using Image J.

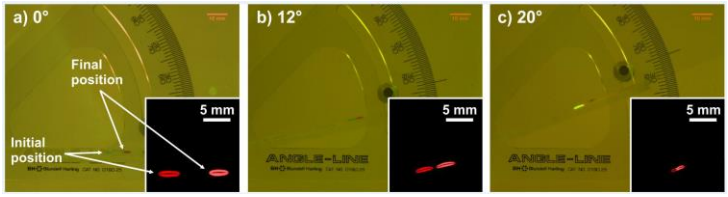

Fig. 3. Overlaid still photographs of droplet translation at (a) 0º, (b) 12º, and (f) 20º showing both initial and final position of the water droplets. Insets show false-color close-ups used for translation analysis.

4. Results and discussion

This section discusses the results from finding the optimized conditions for the experiment, as well as the experimental results, which are compared against the numerical results. To test the efficacy of the numerical simulation built, a parametric study was performed by varying the width, volume and contact angle.

Because of the short-lived hydrophilicity of a plasma-enhanced channel, which we have observed experimentally and reported by Hemmilä et al. (2012), we investigated the use of PVP-treatment, as mentioned in the previous section. Using a goniometer (KSV Instruments), we found that the PVP-treated surface exhibited a more sustained hydrophilicity. As shown in Fig. 4, the contact angle of a sessile water droplet measured on a PVP-treated surface remained at 27º for the first 10 days, while the contact angle measured on the plasma-enhanced surface increased by 25 º. Hemmilä et al. (2012) reported lower contact angle values, ranging from 16 º – 22 º during the first seven days. Nevertheless, compared to using only plasma-treatment, we achieved very much lower contact angle values when PVP-treatment was incorporated. The plasma-enhanced surface continues to show increased contact angle as days progressed, with the highest

recorded at 114^{o} on day-14, while the contact angle for the PVP-treated surface increased to only 36^{o}. In comparison, the highest contact angle over the course of six months reported by Hemmila et al. (2012) was ~ 22 ^{o}.

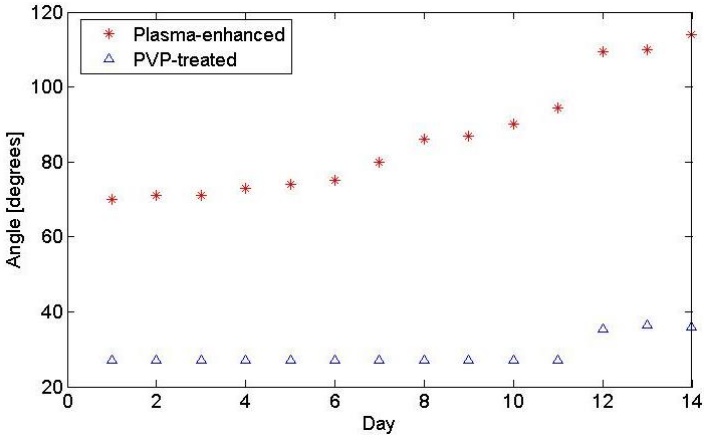

Fig. 4. Contact angle measurements of sessile water droplets on plasma-enhanced and PVP-treated PDMS surfaces.

Besides optimizing the hydrophilic channel, the effect of droplet volume on propulsion distance was studied. On a 1 mm wide PVP-treated channel, propulsion of equal volumes of water and EtOH ranging from 0.2 – 2.1 µl was tested on a horizontal plane. Our findings showed that propulsion distance increases as volume increases from 0.2 µl to 1.0 µl, as shown in Fig. 5. Beyond 1.0 µl, the propulsion distance decreased erratically. We believe that this could be attributed to the overflow of the larger droplet outside the bounds of the hydrophilic channel, as observed experimentally. (Seemann et al., 2005) reported a similar phenomenon, where they

observed an overspill of the droplet outside the contact lines as the droplet volume is increased. Because of the increased footprint, the surface area becomes larger, hence an increased viscous resistance.

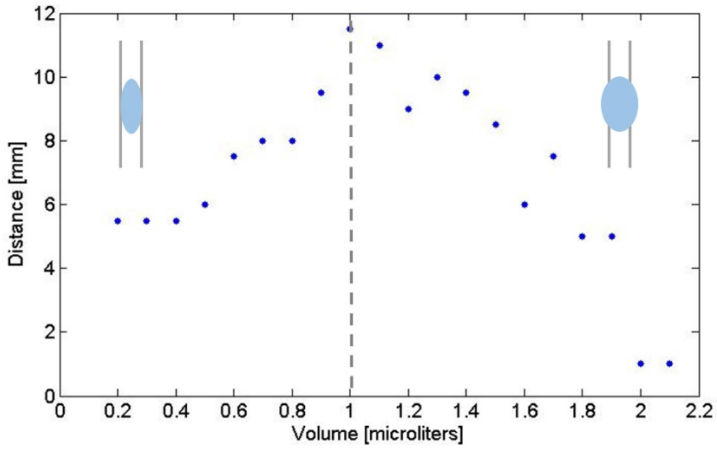

Fig. 5. Plot of propulsion distance using various droplet volumes on a 1 mm wide channel.

Based on the optimized hydrophilic channel and droplet volume, we proceeded with the experiment of propulsion on an incline. Our experimental results showed the highest translation of ~ 10 mm at both 0º and 4º. Subsequent translations at 4º increments showed a linear downward trend, with zero translation at 24º. The experiment for each angle was repeated four times. By taking the average of the traveled distances, the standard deviation for every angle tested was computed. Following that, the error bar for each measurement was obtained, as shown in Fig. 6.

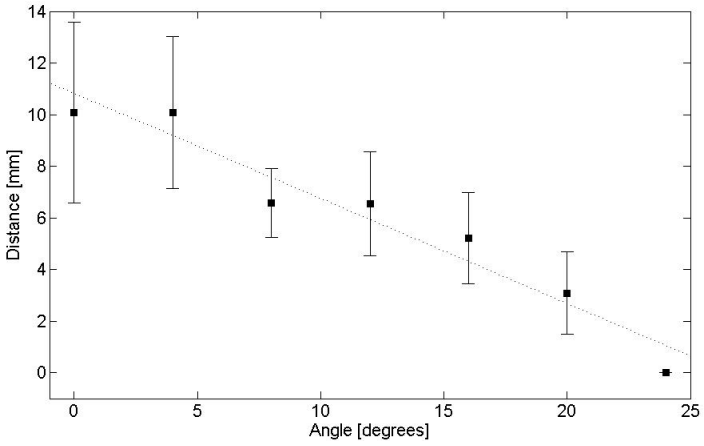

Fig. 6. Plot of distance the water droplet translates on the PDMS substrate for angles starting from 0^o to 24^o, with increments of 4^o.

To further validate our experimental observations, the governing second-order partial differential equations, as detailed in the Section 2, were solved in COMSOL, a commercial Finite Element package able to solve general partial differential equations. The governing equations are first expressed in their weak form and the solution approximated by a trial function using quadratic Lagrange shape functions. COMSOL then uses the Galerkin method whereby the test functions correspond to the shape functions to generate a system of algebraic equations which can then be solved to generate the numerical solution. We found in our case that a mesh resolution of 5,000 elements was sufficient to generate a mesh independent solution. Note that we assumed Dirichlet boundary conditions at both ends where h_c is set to h^* at both ends of the domain and h_1 is set to 0 at the left-hand boundary and h_c at the righ-hand boundary leading to a concentration of 0 and 1, respectively. Natural boundary conditions apply for the pressure.

The input parameters included: $\mu = 0.001$ Pa.s, $\rho = 1000$ kg/m^3, $g = 9.8$ m/s^2, $D = 3 \times 10\text{-}6$ m^2/s, and $h^* = 0.02$. Also, for V = 1 µl, w = 1 mm, $\theta_o = 35^o$, we find $h_o = 0.5$ mm, and $l_o = 2R_o = 3.8$ mm.

Considering the initial coalescence of the two droplets shown in the video, it is clear that only a small portion of the EtOH droplet actually interacted with the water droplet. This portion is *a-priori* unknown but is visibly small. To capture this initial condition we set the EtOH concentration, c = 1 past a distance X_c and c = 0 everywhere else. In other words: $h = h_1$ for $X > X_c$ and $h_1 = 0$ otherwise. The choice $X_c = 94\%$ of the initial droplet radius gave the best match to experimental results. Fig. 7 compares the numerical and experimental results for a substrate inclination angle of 10^o.

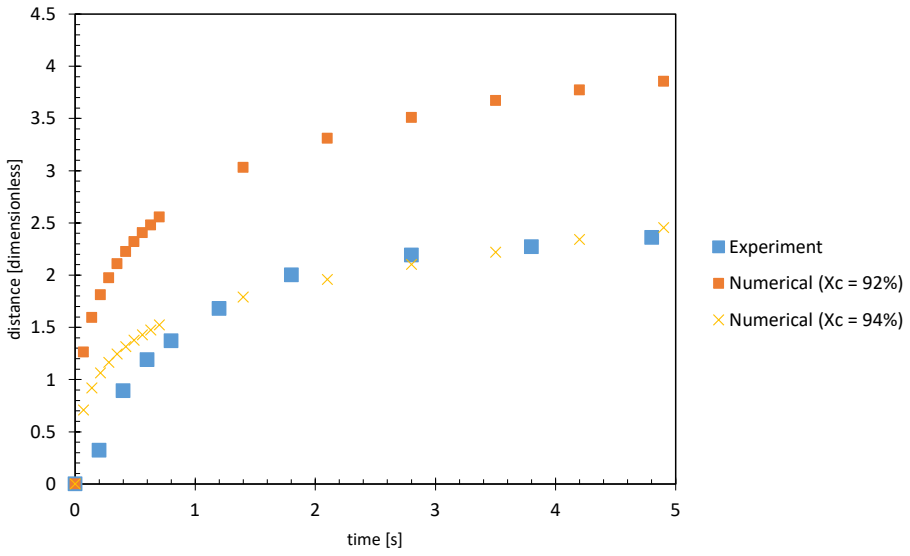

Fig. 7. Comparison of the distance travelled measured experimentally and computed numerically. The y-axis shows the distance travelled normalized by the initial droplet length.

For X_c = 94%, the trend predicted by the numerical simulation is shown to be in good agreement with experimental results although the simulation appears to slightly over-predict the initial droplet velocity. The sensitivity of the numerical simulation to the parameter X_c is also illustrated on Fig. 7 where it can be seen that the smaller X_c corresponding to a larger amount of ethanol in the droplet lead to a larger distance travelled and a larger initial velocity.

To determine the distances traveled from our simulation, we analyzed the centers of gravity, X_{cg} through

$$X_{cg} = \frac{\int_0^L \int_{\frac{-w}{2}}^{\frac{w}{2}} (h - h^*) x \, dy \, dx}{\int_0^L \int_{\frac{-w}{2}}^{\frac{w}{2}} (h - h^*) \, dy \, dx}. \quad (16)$$

Fig. 8. shows how the difference between the position of the centre of gravity computed numerically and the total distance travelled measured experimentally (see Fig. 6) varies with time. For all but the steepest inclined surface (24^o inclination), the numerical results are seen to tend towards 0 indicating that the numerical results tend towards the experimental ones. Because the numerical model does not include the effect of hysteresis which would in practice generate an additional force resisting the motion, the numerical results are seen to overshoot slightly the experimentally observed distance travelled. This is particularly obvious for the flat surface (0^o inclination) for which hysteresis would be the only resistive force beside viscous dissipation. For the most inclined surface of 24^o inclination, the model still predict the motion of the droplet whilst the droplet could not be actuated experimentally. We attribute this difference again to hysteresis which is not included in the numerical model.

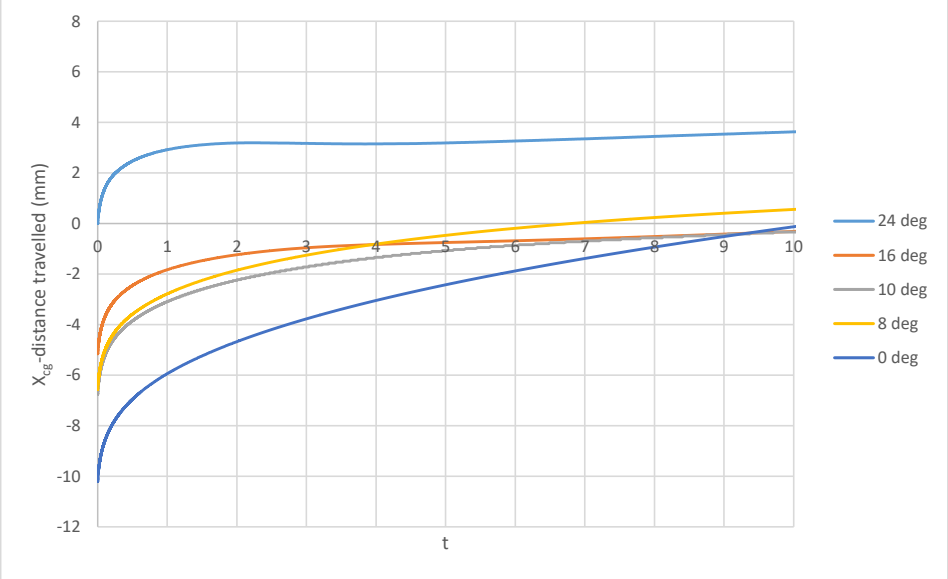

Fig. 8. Comparison between experimental and numerical results for distance traveled.

From the numerical simulation, the predicted distances until t = 2.5 s using various channel widths, droplet volumes and droplet contact angles were analyzed using the X_{cg} function to yield non-dimensional center of gravity values as a function of time, as shown in Fig. 9.

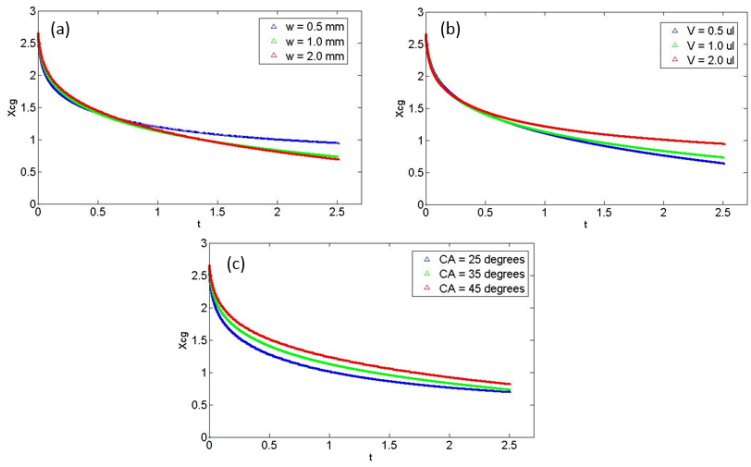

Fig. 9. Center of gravity analysis for distance traveled at 8° incline through varying (a) width, (b) volume, and (c) contact angle.

The distance traveled decreases as channel width decreases, as shown in Fig. 9(a). As droplet volume is decreased, however, the distance traveled increased, as shown in Fig. 9(b). All else equal, when the channel width is smaller or when the droplet volume is larger, we may assume that the droplet becomes more elongated within a channel. This may give rise to additional capillary stresses that may have exceeded Marangoni stress, hence the likeliness of not being displaced very far. It also suggests that a longer slug has a smaller Marangoni effect, hence a smaller driving force resulting in a smaller distance traveled. Fig. 9(c) shows that a droplet with a lower contact angle, or a more hydrophilic droplet, travels further. A vectorial representation of two droplets of equal volume with contact angles $\theta_1 < \theta_2$ as shown in Fig. 10, may aid in understanding this phenomenon. The net force for droplet 1 is $df^1 = df_a^1 - df_r^1$; similarly, the

net force for droplet 2 is $df^2 = df_a^2 - df_r^2$. For the smaller contact angle, θ_1 the driving net force is larger, hence the droplet travels further.

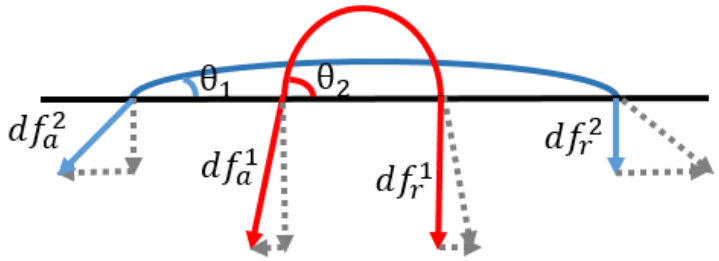

Fig. 10. A diagram representing contact angles, with $\theta_1 < \theta_2$, and their corresponding vector components.

Fig. 11 shows the dimensionless simulation results of not only the distance traveled, but also the droplet morphology as time progresses. The latter is advantageous especially when it is difficult to determine droplet height from image processing; for example, when small volumes are used. The height of a water droplet in a smaller width channel is lower than that in a larger width channel, as shown in Fig. 11(a). The final length, however, is larger. This is simply a consequence of mass conservation in a narrower channel. Fig. 11(b) shows that a 2.0 µl droplet, which is more elongated, travels less than a 0.5 µl droplet. Fig. 11(c) shows that a droplet with a higher contact angle has a higher centerline height and travels less compared to a droplet with a lower contact angle.

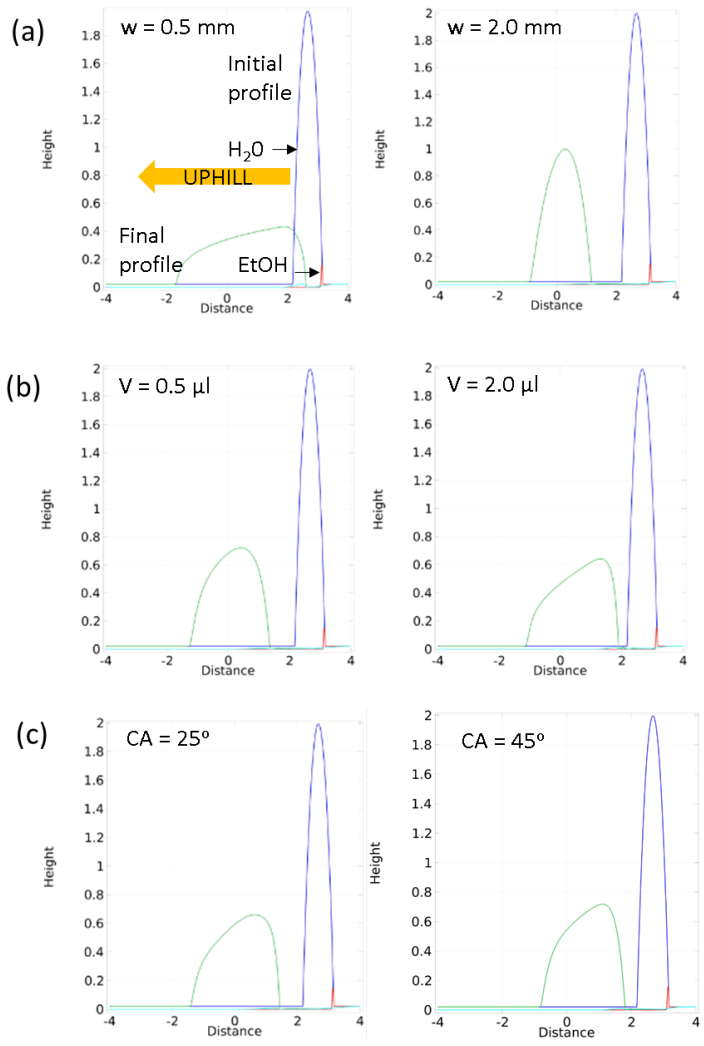

Fig. 11. Dimensionless COMSOL simulation results for 4° incline and t = 5.5 s from varying (a) width, (b) volume, and (c) contact angle. Uphill translation is represented by droplet movement from right to left.

Commented [MS1]: Are you sure this is in seconds?

5. Conclusions

We have successfully shown the self-propulsion of a 1 µl droplet up an incline on a hydrophilic stripe fabricated on a piece of flat PDMS that has undergone oxygen plasma and PVP treatment. The distances traveled by the droplet as a function of angle of incline ranging from 0^o to 24^o were measured. We found that the distance traveled followed a linearly decreasing trend as angle was increased, before reaching zero at 24^o. Numerical solutions generated in COMSOL, which included capillary forces confined within a narrow stripe, as well as gravitational force, validated our experimental observations. Our studies suggest that gravitational pull and contact angle hysteresis overcomes Marangoni force at ~ 24^o, hence the sliding of the droplet downhill. In summary, we have demonstrated a feasible method to move a droplet up an incline through self-propulsion, and developed a numerical simulation that allows for the understanding of the underlying physical principles and the prediction of distance traveled and droplet morphology through varying key experimental variables: width, volume and contact angle.

Acknowledgments

The authors would like to thank Patrick Geoghegan, Helen Devereux and Gary Turner for their technical assistance. Financial support was provided by the Marsden Fund (Grant number UOC1104) administered through the Royal Society of New Zealand.

References

Bain, C.D., Burnett-Hall, G.D., Montgomerie, R.R., 1994. Rapid motion of liquid drops. Nature 372, 414–415.

Brochard, F., 1989. Motions of droplets on solid surfaces induced by chemical or thermal gradients. Langmuir 5, 432–438.

Chandesris, B., Soupremanien, U., Dunoyer, N., 2013. Uphill motion of droplets on tilted and vertical grooved substrates induced by a wettability gradient. Colloids Surf. Physicochem. Eng. Asp. 434, 126–135.
Chaudhury, M.K., Whitesides, G.M., 1992. How to make water run uphill. Science 256, 1539–1541.
Darhuber, A.A., Davis, J.M., Troian, S.M., Reisner, W.W., 2003. Thermocapillary actuation of liquid flow on chemically patterned surfaces. Phys. Fluids 1994-Present 15, 1295–1304.
Ding, X., Li, P., Lin, S.-C.S., Stratton, Z.S., Nama, N., Guo, F., Slotcavage, D., Mao, X., Shi, J., Costanzo, F., Huang, T.J., 2013. Surface acoustic wave microfluidics. Lab. Chip 13, 3626–3649.
Dos Santos, F.D., Ondarçuhu, T., 1995. Free-running droplets. Phys. Rev. Lett. 75, 2972–2975.
Ford, M.L., Nadim, A., 1994. Thermocapillary migration of an attached drop on a solid surface. Phys. Fluids 1994-Present 6, 3183–3185.
Greenspan, H.P., 1978. On the motion of a small viscous droplet that wets a surface. J. Fluid Mech. 84, 125–143.
Hemmilä, S., Cauich-Rodríguez, J.V., Kreutzer, J., Kallio, P., 2012. Rapid, simple, and cost-effective treatments to achieve long-term hydrophilic PDMS surfaces. Appl. Surf. Sci. 258, 9864–9875.
Kim, S.H., Moon, J.-H., Kim, J.H., Jeong, S.M., Lee, S.-H., 2011. Flexible, stretchable and implantable PDMS encapsulated cable for implantable medical device. Biomed. Eng. Lett. 1, 199–203.

Moon, H., Cho, S.K., Garrell, R.L., Kim, C.-J. "CJ," 2002. Low voltage electrowetting-on-dielectric. J. Appl. Phys. 92, 4080–4087.
Nock, V., Muller, Y., Sellier, M., Verdier, C., 2013. Biochemical sensing assays based on coalescence-induced self-propulsion digital microfluidics, in: 2013 Seventh International Conference on Sensing Technology (ICST). Presented at the 2013 Seventh International Conference on Sensing Technology (ICST), pp. 67–70.
Piruska, A., Nikcevic, I., Lee, S.H., Ahn, C., Heineman, W.R., Limbach, P.A., Seliskar, C.J., 2005. The autofluorescence of plastic materials and chips measured under laser irradiation. Lab. Chip 5, 1348–1354.
Seemann, R., Brinkmann, M., Kramer, E.J., Lange, F.F., Lipowsky, R., 2005. Wetting morphologies at microstructured surfaces. Proc. Natl. Acad. Sci. U. S. A. 102, 1848–1852.
Sellier, M., Nock, V., Gaubert, C., Verdier, C., 2013. Droplet actuation induced by coalescence: Experimental evidences and phenomenological modeling. Eur. Phys. J. Spec. Top. 219, 131–141.
Sellier, M., Nock, V., Verdier, C., 2011. Self-propelling, coalescing droplets. Int. J. Multiph. Flow 37, 462–468.
Smith, M.K., 1995. Thermocapillary migration of a two-dimensional liquid droplet on a solid surface. J. Fluid Mech. 294, 209–230.
Vorobyev, A.Y., Guo, C., 2010. Water sprints uphill on glass. J. Appl. Phys. 108, 123512.
Wu, Y., Saito, N., Nae, F.A., Inoue, Y., Takai, O., 2006. Water droplets interaction with super-hydrophobic surfaces. Surf. Sci., Berlin, Germany: 4–9 September 2005 Proceedings of the 23th European Conference on Surface Science 600, 3710–3714.

Yao, X., Bai, H., Ju, J., Zhou, D., Li, J., Zhang, H., Yang, B., Jiang, L., 2012. Running droplet of interfacial chemical reaction flow. Soft Matter 8, 5988–5991.
Yarin, A.L., Liu, W., Reneker, D.H., 2002. Motion of droplets along thin fibers with temperature gradient. J. Appl. Phys. 91, 4751–4760.
Yeo, L.Y., Chang, H.-C., 2005. Static and spontaneous electrowetting. Mod. Phys. Lett. B 19, 549–569.
Yeo, L.Y., Friend, J.R., 2014. Surface Acoustic Wave Microfluidics. Annu. Rev. Fluid Mech. 46, 379–406.
Zeiger, A.S., Hinton, B., Van Vliet, K.J., 2013. Why the dish makes a difference: Quantitative comparison of polystyrene culture surfaces. Acta Biomater. 9, 7354–7361.
Zhang, J., Han, Y., 2007. Shape-gradient composite surfaces: water droplets move uphill. Langmuir 23, 6136–6141.